The Open Journal of Astrophysics
Preprint typeset using LaTeX style openjournal v. 09/06/15

CONNECTING HALOES AND GALAXIES TO THEIR X-RAY EMISSIONS WITH AN EMPIRICAL MODEL OF HOT GAS AND ACTIVE GALACTIC NUCLEI

Johan Comparat[1]
[1]Max-Planck-Institut für extraterrestrische Physik (MPE), Gießenbachstraße 1, D-85748 Garching bei München, Germany
(Dated: August 26, 2025)
submitted

ABSTRACT

This article presents the construction and validation of an X-ray empirical model applied to simulated haloes and the galaxies therein.
Keywords: Large-scale structure, X-ray, galaxies

1. INTRODUCTION

The SRG/eROSITA telescope (Predehl et al. 2021; Sunyaev et al. 2021) gathered soft X-ray photons over half of the sky providing, among other, a new comprehensive view of the extra-galactic large scale structure observed in X-rays (Comparat et al. 2025, , C25 hereafter). In this article, we focus on upgrading the active galactic nuclei model from Comparat et al. (2019, 2023) and the hot gas model from Comparat et al. (2020); Seppi et al. (2022).

2. LIGHT CONE DESCRIPTION

We use the Uchuu simulation (Ishiyama et al. 2021) and the UniverseMachine model (Behroozi et al. 2019; Aung et al. 2023). The DM-only simulation is made of 12 800^3 particles in a cube of length $2h^{-1}$Gpc, corresponding to particles with a mass of $3.27 \times 10^8 h^{-1} M_\odot$. We create a full sky light up to redshift $z \sim 6$ cone by replicating the box (8x8x8 times) using its periodic boundary condition following Comparat et al. (2020). We use 31 snapshots to create shells in the light cone. They are at redshifts 0.00, 0.02, 0.05, 0.09, 0.14, 0.19, 0.25, 0.30, 0.36, 0.43, 0.49, 0.56, 0.63, 0.70, 0.78, 0.86, 0.94, 1.03, 1.12, 1.22, 1.32, 1.43, 1.54, 1.65, 1.77, 1.90, 2.03, 2.17, 2.31, 2.46, 2.62, 2.78, 2.95, 3.13, 3.32, 3.61, 3.93, 4.27, 4.63, 5.15, 5.73.

2.1. *Foregrounds and backgrounds*

We use the same model for the diffuse and resolved foreground and the diffuse background as Comparat et al. (2020); Seppi et al. (2022). We re-generate events

⋆ E-mail: comparat@mpe.mpg.de

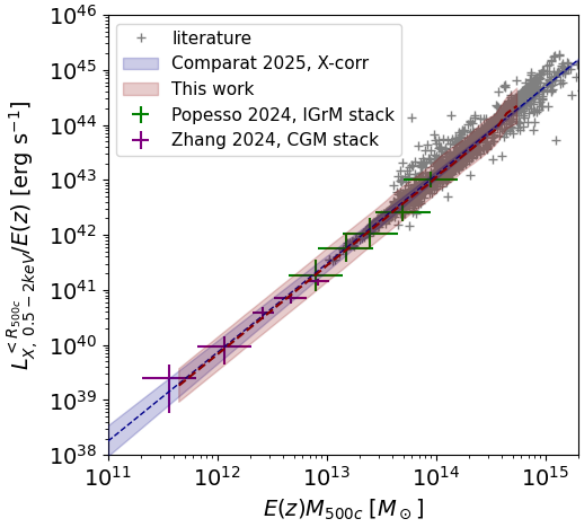

Figure 1. Scaling relation between dark matter halo mass (500c) and X-ray luminosity in the 0.5-2 keV band of the mock catalog (red shaded area and red dashed line). It is made using a light cone shell around redshift of z=0.3. It is by construction in agreement with the recent stacking and cross-correlation analysis of Comparat et al. (2025, blue dashes and shaded area). It agrees well with stacking experiments at low halo masses (Zhang et al. 2024, in purple), in the group regime (Popesso et al. 2024, in green) and with the variety of literature measurements for individual groups and clusters (Lovisari et al. 2015, 2020; Mantz et al. 2016; Adami et al. 2018; Schellenberger & Reiprich 2017; Bulbul et al. 2019; Liu et al. 2022a; Bulbul et al. 2024, in grey crosses).

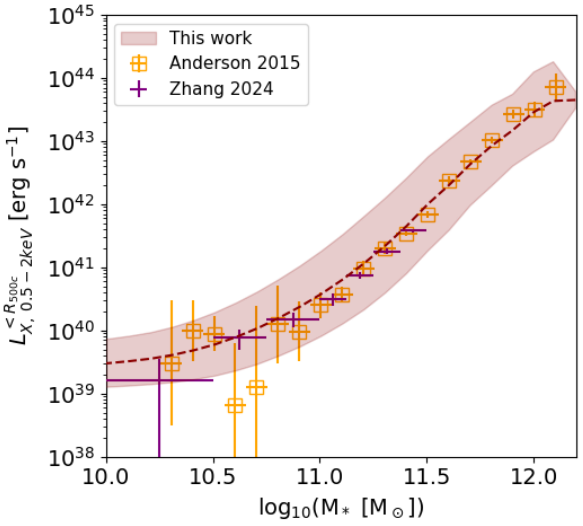

Figure 2. Scaling relation between stellar mass and luminosity in the 0.5-2 keV band. It is made using a light cone shell around redshift of z=0.3. The stellar mass is that predicted by the UniverseMachine model independently of the X-ray luminosity. The red dashes and contours is a prediction of the model, which is in excellent agreement with observations from Anderson et al. (2015, in orange) and Zhang et al. (2024, in purple).

3. X-RAY PREDICTION FOR THE HOT GAS

```
t_sim_gal['upid']==-1)&(t_sim_gal['Mvir']>=5e11)
M500c>1e11
```

The virial mass are converted to 500c with the Ishiyama et al. (2021) mass concentration relation (directly calibrated on Uchuu).

3.1. *luminosity and temperature*

We take a different approach from Comparat et al. (2020) where the scaling relation (and its scatter) is predicted from the covariance matrix. We use the best-fit scaling relation between halo mass and soft X-ray luminosity obtained by Comparat et al. (2025, sample 10.5)

$$\log_{10}(L_X E(z)^{-2}\ [erg\ s^{-1}]) = 44.7 + 1.61(\log_{10}(M_{500c}/M_\odot) - 15) \quad (1)$$

with a scatter of σ_{L_X} =0.3. The parameters of the scaling relation can easily be changed giving more flexibility to the model. The scaling relation obtained is shown in Fig. 1. It agrees well with stacking experiments at low halo masses (Zhang et al. 2024), in the group regime (Popesso et al. 2024). It is in good agreement with observations reported in the literature (Lovisari et al. 2015, 2020; Mantz et al. 2016; Adami et al. 2018; Schellenberger & Reiprich 2017; Bulbul et al. 2019; Liu et al. 2022a; Bulbul et al. 2024).

The stellar mass is not used like in Seppi et al. (2022) to correct the scaling relation to extend to lower halo masses. In this approach, we predict the relation between stellar mass and X-ray luminosity. We compare the obtained predicted relation to Anderson et al. (2015) and Zhang et al. (2024). The comparison shows excellent agreement, see Fig. 2.

For the temperature, we use

$$\log_{10}(kT\ E(z)^{-2/3}[keV]) = 0.6\log_{10}(M_{500c}/M_\odot) - 8 \quad (2)$$

with a scatter of σ_{kT} =0.2. The covariance between the two is

```
[[sigma_kT**2, rho*sigma_kT*sigma_LX ],
[rho*sigma_kT*sigma_LX, sigma_LX**2]]
```

with ρ =0.95. We draw a normal random variable from this matrix to add correlated scatter in the observables. Future improvement include using the complete mass dependent covariance matrix predicted by hydrodynamical simulations (e.g. Flamingo, Jamal et al. in prep). The scaling relation obtained is shown in Fig. 3. This line is in good agreement with observations of galaxy groups and clusters (Lovisari et al. 2015; Mantz et al. 2016; Adami et al. 2018; Bulbul et al. 2019; Lovisari et al. 2020), with the stacked groups from Toptun et al. in submitted and with the measurement of our own Milky Way from (Ponti et al. 2023).

We compute K-correction on a fine grid of redshift and temperature. With that we convert the intrinsic luminosity into an unabsorbed observed flux. Finally, we add absorption using the Nh4PI tabulated skymap (HI4PI Collaboration et al. 2016). The absorption is tabulated for three temperatures: 0.5, 1 and 2keV. For haloes hotter than 1.5keV, we use the 2keV approximation, for the ones in the range 0.7 to 1.5 keV the 1keV approximation. and the cooler ones with the 0.5 keV approximation.

The obtained logN-logS (unabsorbed 0.5-2 keV flux) is somewhat bright but its shape follows that of observations (Fig. 4). The mock is brighter than observations. This feature was addressed previously by using a hydrostatic mass bias value of 0.8. In this iteration, we prefer to avoid adding more parameters since we are interested in the lower mass range where that bias is not applicable due to differences in the measurement procedures.

3.2. *X-ray profiles*

We use the method of Comparat et al. (2020) to create a library of profile. It represents the diversity of exiting profile shapes encountered in observations. The profile shapes are randomly assigned to haloes.

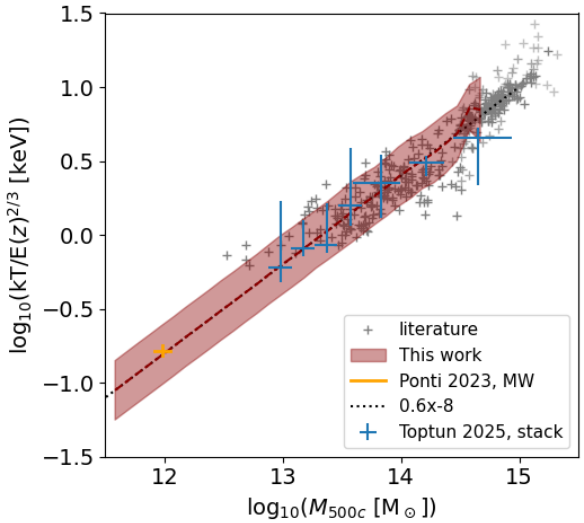

Figure 3. Scaling relation between dark matter halo mass (500c) and temperature of the mock catalog (red shaded area and red dashed line). It is made using a light cone shell around redshift of z=0.3. The model prediction is in good agreement with observations of galaxy groups and clusters (Lovisari et al. 2015; Mantz et al. 2016; Adami et al. 2018; Bulbul et al. 2019; Lovisari et al. 2020), with the stacked groups from Toptun et al. in submitted and with the measurement of our own Milky Way from (Ponti et al. 2023).

From Sanders et al. (2025), we extract a distribution of ellipticities in four broad bins to obtain the relative frequencies of ellipticities in observations for the S2 volume-limited sample from Seppi et al. (2024). The number of ellipticity values one may use directly scales with the number of images one has to generate. In Comparat et al. (2020); Seppi et al. (2022), we created an image for each source, which was heavy in disk usage and and was proven not to be a key information to model the selection function (Seppi et al. 2022; Clerc et al. 2024). So we take here a path where less images are created. We sample 2,796 profiles and 4 ellipticities for each redshift shell (22), totaling 246,048 tabulated images representing hot gas profiles up to redshift 1.5.

The ellipticities (denoted ϵ) take four discrete values: [0.55, 0.65, 0.75, 0.85] with fractions of [0.22, 0.30, 0.25, 0.23] representing the fraction of clusters with a given ellipticity value.

The ellipticity of the images simulated is set at 0.75, the average of the eRASS:1 cluster ellipticities (Sanders et al. 2025).

EVENT GENERATION

We re-cast the simput files into the eROSITA sky tiles and merge them to make a single simput per source type in each field. Given the mean exposure time of the field, a flux cut is applied to only simulate sources that will generate photons. Indeed, image simulations are more intensive, so one should strive for efficiency instead of looping over all haloes and finding out that they emit no events in the time laps simulated.

We use a synthetic eRASS:8 attitude file to generate a superset of events (containing the observed eRASS:1 or eRASS:5 GTI). For every selection function exercise, the event files are then tailored (GTI filtering) for the specific need. Fig. 5 illustrates the generated events for the hot haloes.

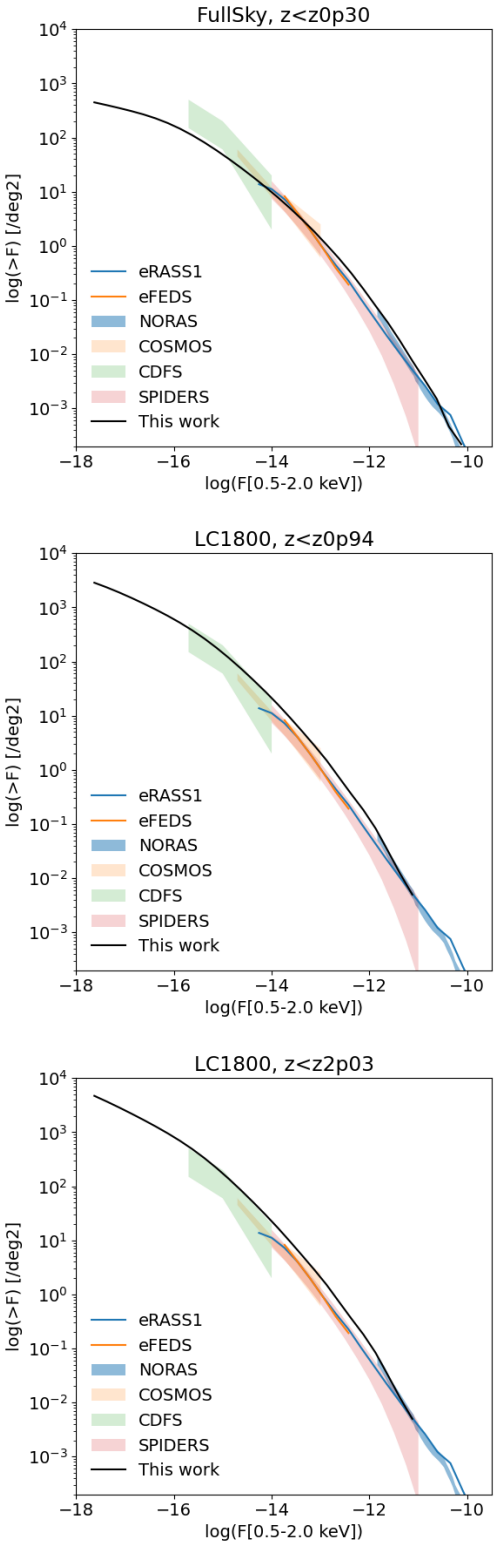

Figure 4. logNlogS. Number density of sources brighter than and observed flux in the 0.5-2 keV band.

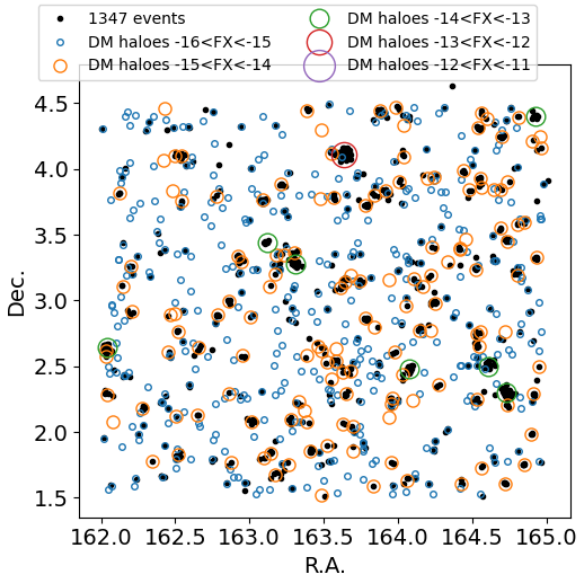

Figure 5. Simulated events for the sky tile number 164087. Haloes are split as a function of their total flux (within 2 times R_{500c}, the boundary of the simulated image).

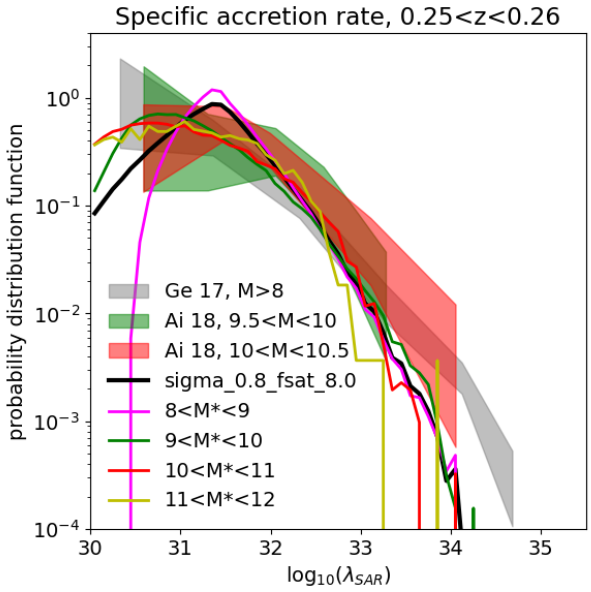

Figure 6. Distribution of specific accretion rate at z=0.25. The model prediction is shown (with colored solid lines) for four stellar mass bins (8, 9, 10, 11, 12). It is in fair agreement with observations (shaded areas) from Georgakakis et al. (2017, Ge17), Aird et al. (2018, Ai18)

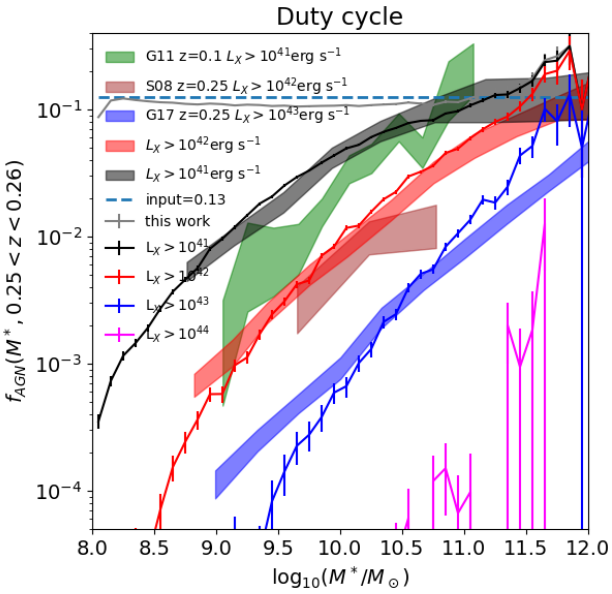

Figure 7. Duty cycle at z=0.25. Fraction of galaxies with a model active galactic nucleus as a function of stellar mass, provided an input maximum duty cycle of 11% taken from (Georgakakis et al. 2017). The model prediction is shown (with colored solid lines with uncertainties) for four hard X-ray (2-10 keV) luminosity thresholds (41, 42, 43, 44) and the complete sample (grey). It is in fair agreement with observations (shaded areas) from Georgakakis et al. (2017, Ge17), Shi et al. (2008, S08), Georgakakis et al. (2011, G11).

4. AGN MODEL

We use the parametrization from Comparat et al. (2019) and Liu et al. (2022b) with the best combination of parameters found in Comparat et al. (2023). The scatter in the abundance matching relation between stellar mass and hard X-ray luminosity function from Aird et al. (2015) is $\sigma_{AGN} = 0.8$ and the satellite fraction is set at $f_{sat} = 8\%$. The obscuration model is as in Comparat et al. (2019).

The specific accretion rate distribution (SAR), defined by

$$\lambda_{SAR} = \frac{L_X^{2-10\,\mathrm{keV}}}{M^*}, \quad (3)$$

is shown in Fig. 6. It directly reflects the scatter in the abundance matching relation. So, by construction, this model can not recover the double power-law behavior observed, in particular at the high SAR end, see observations from Georgakakis et al. (2017); Aird et al. (2018). The model agrees fairly well with the observations in the range 30 to 33.

The duty cycle obtained is illustrated in Fig. 7. It follows well observations from Georgakakis et al. (2017); Shi et al. (2008); Georgakakis et al. (2011).

The obtained stellar mass function of galaxies hosting AGN is shown in Fig. 8. The shape of the host galaxy stellar mass function is in fair agreement with the model from Bongiorno et al. (2016).

This model starts from the hard X-ray luminosity function ans predicts via an obscuration model a soft X-ray luminosity function, shown in Fig. 9. The predicted unobscured soft X-ray luminosity function is in fair agreement with the measurements from Hasinger et al. (2005).

Finally, we find that the predicted number density of sources per square degree as a function of soft X-ray flux (logN-logS) is in fair agreement with observations (Mateos et al. 2008; Georgakakis et al. 2008), see Fig. 10. The low number of very bright sources comes from the luminosity function used at low redshift. At the faint end, extending beyond redshift 4, provides a prediction closer to the obser-

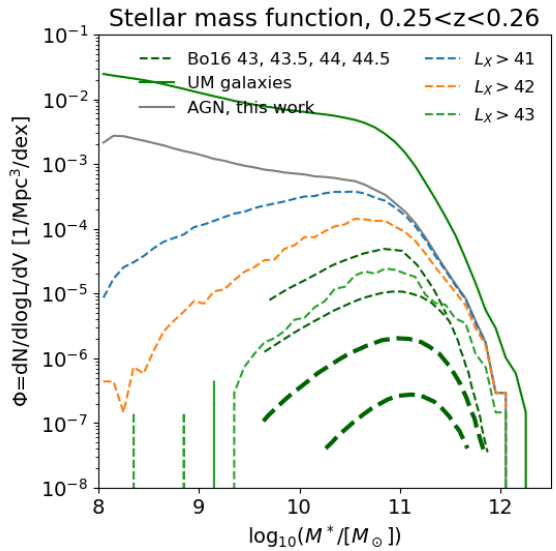

Figure 8. Stellar mass function at z=0.25. Number density of galaxies with a model active galactic nucleus as a function of stellar mass. The model prediction is split (with colored dashes lines) for three hard X-ray (2-10 keV) luminosity thresholds (41, 42, 43) and the complete sample (grey). Observations (green dashes) from Bongiorno et al. (2016, Bo16) are shown for four luminosity thresholds 43, 43.5, 44, 44.5. The complete model galaxy population is shown with the solid green line.

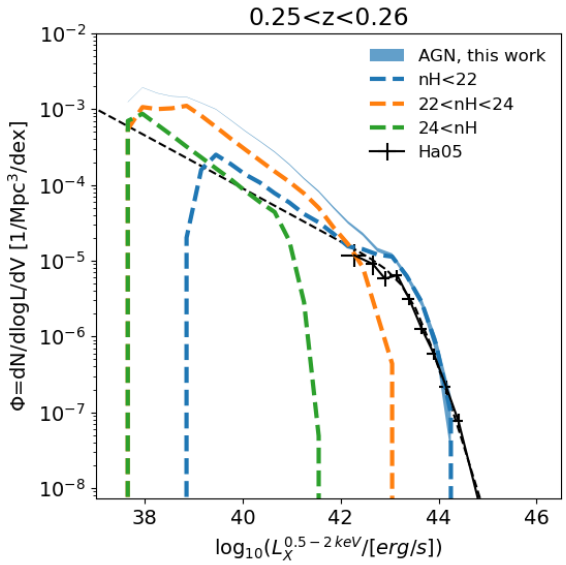

Figure 9. Soft X-ray luminosity function at z=0.25. Number density of AGN as a function of soft X-ray luminosity. The model prediction is split (with colored dashes lines) in three obscuration bins (delimited by 20, 22, 24, 26, unobscured, obscured, thick obscured) and the complete sample (blue). Observations (black crosses) and their best fit model (black dashes) from Hasinger et al. (2005, Ha05) are shown. The unobscured luminosity function (blue dashes) is in good agreement with observations.

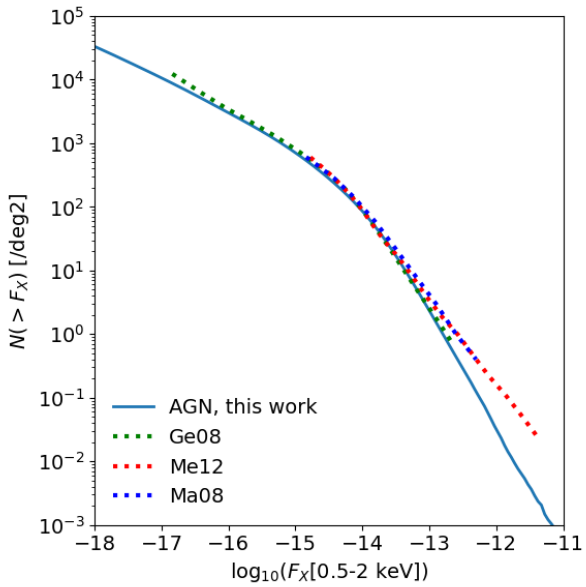

Figure 10. logN-logS. Number density of sources per square degree as a function of soft X-ray flux with all AGN up to redshift 4. Observations and their best fit model from Mateos et al. (2008, Ma08) and Georgakakis et al. (2008, Ge08) are shown with dotted lines. The model for the compilation presented by Merloni et al. (2012, Me12) is shown in red dots.

vations.

This incarnation of the AGN model from Comparat et al. (2019), using the Uchuu simulation and UniverseMachine galaxy model together with parameters from Comparat et al. (2023), seems to describe well to first order the AGN population (up to redshift of 4).

EVENT GENERATION

To generate events, we limit the catalogs to sources brighter than $F_X^{0.5-2\mathrm{keV}} > 10^{-16}$ erg cm^{-2} s^{-1}. We tabulate X-ray spectra using the xspec models described in Liu et al. (2022b). Events are then generated following an idealized eRASS:8 attitude file.

5. MERGING EVENT FILES

To characterize how sources are detected, different simulated experiments are needed. For each eROSITA field, we have five sets of event files: hot gas, active galactic nuclei, stars, particle background and true observed events.

5.1. *Purity determination*

Purity is determined is a completely controlled environment. We merge all simulated event files, trimmed to match the exposure time of the real observations on the same field. We then run the source detection algorithm as in the observations and quantify the purity of the samples detected.

6. CROSS-CORRELATION BENCHMARK

We predict the intrinsic cross-correlation between central and satellite galaxies in narrow redshift bins and events in the 0.5-2 keV band coming from the hot gas, AGN and background model. To avoid spurious correlation due to the box replication, We filter events that come from sources located in the first replication of the simulation (with the src id) and add different number of background events to fill the required amount of events (the observed event density).

7. SUMMARY

—

REFERENCES

Adami, C., Giles, P., Koulouridis, E., et al. 2018, A&A, 620, A5
Aird, J., Coil, A. L., & Georgakakis, A. 2018, MNRAS, 474, 1225
Aird, J., Coil, A. L., Georgakakis, A., et al. 2015, MNRAS, 451, 1892
Anderson, M. E., Gaspari, M., White, S. D. M., Wang, W., & Dai, X. 2015, MNRAS, 449, 3806
Aung, H., Nagai, D., Klypin, A., et al. 2023, MNRAS, 519, 1648
Behroozi, P., Wechsler, R. H., Hearin, A. P., & Conroy, C. 2019, MNRAS, 488, 3143
Bongiorno, A., Schulze, A., Merloni, A., et al. 2016, A&A, 588, A78
Bulbul, E., Chiu, I. N., Mohr, J. J., et al. 2019, ApJ, 871, 50
Bulbul, E., Liu, A., Kluge, M., et al. 2024, A&A, 685, A106
Clerc, N., Comparat, J., Seppi, R., et al. 2024, A&A, 687, A238
Comparat, J., Eckert, D., Finoguenov, A., et al. 2020, The Open Journal of Astrophysics, 3, 13
Comparat, J., Luo, W., Merloni, A., et al. 2023, A&A, 673, A122
Comparat, J., Merloni, A., Ponti, G., et al. 2025, arXiv e-prints, arXiv:2503.19796
Comparat, J., Merloni, A., Salvato, M., et al. 2019, MNRAS, 487, 2005
Georgakakis, A., Aird, J., Schulze, A., et al. 2017, MNRAS, 471, 1976
Georgakakis, A., Coil, A. L., Willmer, C. N. A., et al. 2011, MNRAS, 418, 2590
Georgakakis, A., Nandra, K., Laird, E. S., Aird, J., & Trichas, M. 2008, MNRAS, 388, 1205
Hasinger, G., Miyaji, T., & Schmidt, M. 2005, A&A, 441, 417
HI4PI Collaboration, Ben Bekhti, N., Flöer, L., et al. 2016, A&A, 594, A116
Ishiyama, T., Prada, F., Klypin, A. A., et al. 2021, MNRAS, 506, 4210
Liu, A., Bulbul, E., Ghirardini, V., et al. 2022a, A&A, 661, A2
Liu, T., Merloni, A., Comparat, J., et al. 2022b, A&A, 661, A27
Lovisari, L., Reiprich, T. H., & Schellenberger, G. 2015, A&A, 573, A118
Lovisari, L., Schellenberger, G., Sereno, M., et al. 2020, ApJ, 892, 102
Mantz, A. B., Allen, S. W., Morris, R. G., & Schmidt, R. W. 2016, MNRAS, 456, 4020
Mateos, S., Warwick, R. S., Carrera, F. J., et al. 2008, A&A, 492, 51
Merloni, A., Predehl, P., Becker, W., et al. 2012, arXiv e-prints, arXiv:1209.3114
Ponti, G., Zheng, X., Locatelli, N., et al. 2023, A&A, 674, A195
Popesso, P., Marini, I., Dolag, K., et al. 2024, arXiv e-prints, arXiv:2411.17120
Predehl, P., Andritschke, R., Arefiev, V., et al. 2021, A&A, 647, A1
Sanders, J. S., Bahar, Y. E., Bulbul, E., et al. 2025, A&A, 695, A160
Schellenberger, G. & Reiprich, T. H. 2017, MNRAS, 469, 3738
Seppi, R., Comparat, J., Bulbul, E., et al. 2022, A&A, 665, A78
Seppi, R., Comparat, J., Ghirardini, V., et al. 2024, A&A, 686, A196
Shi, Y., Rieke, G., Donley, J., et al. 2008, ApJ, 688, 794
Sunyaev, R., Arefiev, V., Babyshkin, V., et al. 2021, A&A, 656, A132
Zhang, Y., Comparat, J., Ponti, G., et al. 2024, A&A, 690, A268

APPENDIX

This paper was built using the Open Journal of Astrophysics LaTeX template. The OJA is a journal which provides fast and easy peer review for new papers in the astro-ph section of the arXiv, making the reviewing process simpler for authors and referees alike. Learn more at http://astro.theoj.org.